Characteristics Study of HEMT using Quantum Transport Model through an Indigenous Program

A Project Report

Submitted by:

Sourjya Mukherjee (2014182)
Kurumoju Deepak (2014189)
Pankaj Gupta (2014038)

in partial fulfillment for the award of the degree of

BACHELOR OF TECHNOLOGY IN

ELECTRONICS AND COMMUNICATION ENGINEERING

DEPARTMENT OF ELECTRONICS AND COMMUNICATION ENGINEERING

NATIONAL INSTITUTE OF TECHNOLOGY SILCHAR,

SILCHAR, ASSAM (INDIA)-788010

May 2024

DECLARATION

We hereby declare that the project entitled "**Characteristics Study of HEMT using Quantum Transport Model through an Indigenous Program**" submitted for the B. Tech. (ECE) degree is our original work and the project has not formed the basis for the award of any other degree, diploma, fellowship, or any other similar titles.

Place: Signature of Students:

Date:

Sourjya Mukherjee (2014182)

Kurumoju Deepak (2014189)

Pankaj Gupta (2014038)

CERTIFICATE

This is to certify that the project titled "**Characteristics Study of HEMT using Quantum Transport Model through an Indigenous Program**" is the bonafide work carried out by **Sourjya Mukherjee (2014182)**,**Kurumoju Deepak (2014189)** and **Pankaj Gupta (2014038)** students of B Tech (ECE) of National Institute of Technology Silchar (An Institute of National Importance under MHRD, Govt. of India), Silchar, Assam, India during the academic year 2023-24, in partial fulfillment of the requirements for the award of the degree of Bachelor of Technology (Electronics and Communication Engineering) and that the project has not formed the basis for the award previously of any other degree, diploma, fellowship or any other similar title.

Place:

Date:

Supervisor: **Dr. Trupti Ranjan Lenka**

Associate Professor,

Department of Electronics & Communications Engineering,

National Institute of Technology Silchar, Assam.

Abstract

This report offers an in-depth exploration of High Electron Mobility Transistors (HEMTs), emphasizing the fundamental principle of two-dimensional electron gas (2DEG) formation. HEMTs, made from Group III-nitride materials, are essential for high-power RF and microwave applications due to their ability to create a 2DEG at the heterointerface. This is achieved by engineering semiconductor layers with different bandgaps, resulting in a potential energy step that confines electrons within a two-dimensional plane. An innovative simulation system, utilizing Kronecker matrices with convolution-based interpolation and gradient clipping, is introduced to solve the Poisson and Schrödinger equations self-consistently. This system provides detailed insights into electron wave functions, electric potential distribution, electron density, Fermi surface energy, and current density distribution within HEMT devices. The initial phase of the project focuses on the mathematical solution of quantum mechanical equations to produce self-consistent results. Experimental results were validated against state-of-the-art Silvaco TCAD simulations. Subsequently, these insights are applied to develop a novel gate-all-around FET structure, with simulation outputs generated using Silvaco TCAD. This research significantly enhances the understanding and optimization of HEMTs, supporting their application in advanced nanoscale electronics.

List of Figures

Table of Contents

Chapter 1

Introduction

In the rapidly evolving landscape of electronic devices and power conversion technologies, High Electron Mobility Transistors (HEMTs) have emerged as pivotal components, offering exceptional high-frequency performance and power handling capabilities. Unlike traditional Metal-Oxide-Semiconductor Field-Effect Transistors (MOSFETs), HEMTs rely on a fundamentally different operational principle—the creation of a two-dimensional electron gas (2DEG) at a heterojunction interface. This unique feature, enabled by carefully engineered material combinations and energy band alignments, empowers HEMTs with unparalleled electron mobility and makes them well-suited for high-power Radio Frequency (RF) and microwave applications.

While MOSFETs have been the cornerstone of silicon technology, their application in high-performance transistors is limited in the context of Group III-nitride materials, such as Gallium Nitride (GaN). The absence of a high-quality gate dielectric comparable to silicon's native oxide (SiO2) has posed a significant challenge. In response, researchers have explored alternative transistor structures like the Metal-Semiconductor Field-Effect Transistor (MESFET) in GaN technology. However, achieving the required doping levels and gate-channel proximity for high-performance, short-channel devices

has proven to be a formidable task.

Enter the HEMT a transformative structure that overcomes these challenges. HEMTs offer a unique blend of attributes, including close gate proximity to the conducting channel, high transconductance, and high drain efficiency. Additionally, their superior characteristics, such as high low-field mobility, maximum drift velocity, and electron sheet densities, render them exceptionally well-suited for demanding high-power RF and microwave applications. The inherent high power per device width of GaN HEMTs translates into smaller, more manufacturable devices with enhanced impedance characteristics, simplifying impedance matching in complex systems.

Furthermore, the emergence of HEMTs owes its inspiration to the exploration of AlGaAs/GaAs quantum wells and superlattices, where the confinement and high concentration of carriers at heterointerfaces were discovered. The HEMT structure effectively harnesses this principle by burying the 2DEG at the heterojunction interface, isolating it from the rough surface, and controlling it through gate-induced band bending.

In addition to exploring the principles and applications of High Electron Mobility Transistors (HEMTs), this paper aims to achieve the following objectives:

- To develop a comprehensive, indigenous simulation software tailored for nanoelectronic devices, particularly HEMTs.
- To Iteratively solve the Poisson and Schrödinger equations to attain a self-consistent solution, crucial for accurate device modeling.
- To Obtain the electric potential profile across the HEMT device, revealing the electrostatics and potential energy landscape.
- To Calculate electron probability densities ($|\psi|^2$) and energy eigenvalues, providing insights into electron behavior and energy levels.

- To Determine the electron concentration distribution within the device.
- To Analyze the current density distribution across the device, shedding light on electron flow and device performance.
- To Extend the model to incorporate quantum transport effects, enhancing simulation accuracy.

By addressing these objectives, this research advances our understanding of HEMTs and contributes valuable simulation tools for nanoelectronic device analysis.

Chapter 2

Literature Review

In the realm of semiconductor physics and nanoelectronic device modeling, Schrödinger's equation elucidates the quantum behavior of electrons within the material, determining energy levels and electron wave functions. Poisson's equation, on the other hand, characterizes electric potential and charge distribution, crucial for understanding the electrostatics within devices. [1] by Neaman et al. provides a foundational understanding of these equations, enabling us to grasp how quantum mechanics and electrostatics influence the behavior of electrons and charge carriers in semiconductor materials. [2] by Morkoç et al is a comprehensive reference work that focuses on Gallium Nitride (GaN)-based semiconductor materials and their applications in electronic and optical devices. The book covers a wide range of topics related to GaN, including electronic and optical processes, device physics, material parameters and practical applications. It served as a valuable resource to this work as it helped understand the intrinsic band properties of the materials that were used in this work.($Al_xGa_{(1-x)}N$ and GaN).

Zarak et al.[3] proposed a physics-based analytical model for p-GaN/AlGaN/GaN High Electron Mobility Transistors (HEMTs) at the 2022 IEEE 19th India Council International Conference (INDICON). This model leverages MATLAB with FlexPDE to

efficiently solve the Schrödinger's equation and Poisson's equation, to arrive at a self consistent solution which are fundamental in understanding the quantum behavior of electrons and electrostatics within the semiconductor material. However the proposed work does not take into account the polarization effect of the materials involved.In contrast to previous papers, the study proposed by Singh et al.[4] utilizes ATLAS, a semiconductor device simulation software, to delve into a comprehensive analysis of the current-voltage (I-V) characteristics in AlN/-Ga2O3 High Electron Mobility Transistors (HEMTs). One noteworthy aspect of this research is its in-depth exploration of Dirichlet and Neumann boundary conditions, shedding light on their intricate roles and implications within the context of semiconductor device modeling.The Ph.D. thesis by G. Leuzzi[5] holds significance in the context of simulating High Electron Mobility Transistor (HEMT) characteristics for AlGaN materials. Notably, the author modified a MATLAB library called "AQUILA" to facilitate the simulation of HEMT device characteristics, particularly in the AlGaN semiconductor material. This thesis is of particular relevance to our work as it provides a clear and detailed explanation of how to solve the Schrödinger's equation through discretization and matrix-based methods.

In conclusion, the reviewed papers, books, and theses have collectively provided valuable insights into the intricate realm of semiconductor physics and the modeling of High Electron Mobility Transistors (HEMTs). These resources have shed light on fundamental equations, such as Schrödinger's equation and Poisson's equation, which govern the behavior of electrons and electrostatics within semiconductor materials. Notably, the proposed methods in these works have been implemented using licensed software tools, highlighting the importance of developing an indigenous and freely accessible program for simulating and modeling HEMT characteristics.

The primary aim of our project is to comprehensively understand the underlying principles of HEMTs, leveraging the knowledge gleaned from these valuable resources. Moreover, we aspire to bridge the gap by creating an indigenous software solution that

stands on par with established models while remaining cost-free. This software will be a valuable asset for researchers and engineers, facilitating the simulation and modeling of HEMT characteristics with ease and accessibility, ultimately advancing the field of semiconductor device research and design.

Chapter 3

Materials and Methodology

3.1 Theory:

3.1.1 Heterojunction Structure:

HEMTs are typically built using semiconductor materials with different bandgap energies, creating what is known as a heterojunction structure. Common material combinations include Gallium Nitride (GaN) or Indium Phosphide (InP) for the channel region and Aluminum Gallium Nitride ($Al_xGa_{(1-x)}As$)) or other materials for the barrier layer. The heterojunction interface plays a crucial role in forming a two-dimensional electron gas (2DEG), which is a key feature of HEMTs. 1st Section

3.1.2 Formation of 2DEG Electron Gas:

The formation of a two-dimensional electron gas (2DEG) in a High Electron Mobility Transistor (HEMT) is a key principle that underlies its high electron mobility and exceptional performance. The formation of the 2DEG is primarily dependent on the energy band alignment at the heterojunction interface between the channel and barrier materials. Here's a detailed explanation of how the 2DEG is formed and its relationship

to electron mobility:

In a HEMT, two different semiconductor materials are used, typically with different bandgap energies. For example, Gallium Nitride (GaN) is often used as the channel material, and Aluminum Gallium Nitride ($Al_xGa_{(1-x)}As$) or similar materials are used as the barrier material. The key to forming a 2DEG lies in creating a conduction band discontinuity (energy step) at the heterojunction interface between these materials.

- The conduction band of the barrier material should be lower in energy than the conduction band of the channel material. This energy difference is the key factor. (Here we are considering all bound electron energy levels to be negative i.e E_c values are negative as they are compared to the energy of an electron in free space)

- This means that the energy difference (ΔE_c) between the conduction band edges of the two materials must be sufficient to create an energy step that confines electrons to the interface. ($\Delta E_c > 0$)

- The result is that electrons accumulate at the heterojunction interface, forming a 2DEG within a narrow region at the interface.

3.1.3 High Electron Mobility:

The high electron mobility associated with the 2DEG in HEMTs arises from the fact that electrons in the 2DEG experience minimal scattering and resistive losses. This is due to:

- The 2DEG's confinement to a narrow interface region, which reduces scattering events and electron-phonon interactions.

- The absence of impurities in the channel region, which further minimizes scattering.

- The relatively high electron mobility of the materials used in the channel region of HEMTs, such as GaN, which inherently supports high electron mobility.

3.2 Material Parameters

3.2.1 BandGap

The ternary alloy of GaN and AlN, $Al_xGa_{(1-x)}$, provides a wide continuous range of bandgap values with a small associated change in the lattice constant. The energy bandgap of $Al_xGa_{(1-x)}As$ is modelled with both a temperature and a compositional dependence. The compositional dependence of the principal bandgap of $Al_xGa_{(1-x)}As$ shows a nonlinear increase of the bandgap with increasing Al-content. It is modelled by the empirical equation 3.1

$$E_g(x) = xE_g(\mathrm{AlN}) + (1-x)E_g(\mathrm{GaN}) - bx(1-x)\,\mathrm{eV} \tag{3.1}$$

with x and b representing the mole-fraction of Al and the bowing parameter, respectively. The values of the bowing parameter still show big inconsistencies in the literature. The temperature dependence of the bandgap is modelled by the empirical Varshni equation 3.2

$$E_g(T) = E_g(0) - \frac{\alpha T^2}{\beta + T}\,\mathrm{eV} \tag{3.2}$$

with α and β being empirical parameters which are given along with other parameters in table 3.1

Table 3.1 Energy bandgaps of AlN and GaN and empirical fitting parameters

Parameter	Value
Bandgap E_g(AlN) [eV]	6.1
Bandgap E_g(GaN) [eV]	3.42
Bowing parameter b	-1
Fitting parameter α	2.15×10^{-3}
Fitting parameter β	1561
EV discontinuity [eV]	$0.85x$

3.2.2 Effective carrier masses

The effective mass for $Al_xGa_{(1-x)}As$ is once again a linear interpolation between the values of AlN and GaN given by eqn 3.3

$$m^*(Al_xGa_{1-x}N) = (1-x)m^*(GaN) + xm^*(AlN) \tag{3.3}$$

effective m* values have been tabulated in table 3.2

Table 3.2 Effective masses of carriers in AlN and GaN (expressed in units of free electron mass m_0)

Carrier	Mass in AlN	Mass in GaN
$m_{\perp,e^-}$ $(=m_{\|\|,e^-})$	0.27 m_0	0.18 m_0

3.2.3 Dielectric constant

The relative dielectric constant of the $Al_xGa_{(1-x)}$ alloy is a linear interpolation between the dielectric constants of the binary alloys GaN and AlN for Al mole fraction x given by eqn 3.4

$$\varepsilon_{Al_xGa_{1-x}N} = 10.28 + 0.03x \tag{3.4}$$

3.2.4 Schottky Barrier

The electron affinity of GaN and AlN are approximately 4.2 eV and 2.05 eV, respectively. By using a linear interpolation between the electron affinities of GaN and AlN the barrier height between an arbitrary metal and the alloy $Al_xGa_{(1-x)}As$ can be calculated with eqns 3.5

$$\phi_{B(\text{metal}-Al_xGa_{1-x}N)} = \phi_m - \chi_{Al_xGa_{1-x}N} \tag{3.5}$$

$$\chi_{Al_xGa_{1-x}N} = \chi_{GaN} + (1-x)\chi_{AlN} \tag{3.6}$$

3.3 Equations:

3.3.1 Poisson's Equation

Poisson's equation describes the distribution of a scalar field, such as the electric potential in electrostatics in a given region of space due to a specified source distribution, such as charge density.

In the context of electrostatics, Poisson's equation relates the Laplacian of the electric potential ($\nabla^2\phi$) to the charge density (ρ) given by 3.7:

$$\nabla^2\phi = -\frac{\rho}{\varepsilon_0} \tag{3.7}$$

where:

- ∇^2 is the Laplacian operator
- ϕ is the electric potential,
- ρ is the charge density, and

- ε_0 is the vacuum permittivity

This equation essentially states that the Laplacian of the electric potential is equal to the negative of the charge density divided by the vacuum permittivity. It quantifies how charges in a given region of space influence the electric potential throughout that region.

3.3.2 Schrodinger's Equation

The time-independent Schrödinger equation (TISE) describes the stationary states of a quantum system. In one dimension, it is given by 3.8:

$$-\frac{\hbar^2}{2m}\frac{d^2\psi(x)}{dx^2} + V(x)\psi(x) = E\psi(x) \tag{3.8}$$

where:

- $\hbar$ is the reduced Planck constant,
- m is the mass of the particle,
- E is the energy eigenvalue,
- $\psi(x)$ is the wave function, and
- $V(x)$ is the potential energy function.

In three dimensions, the TISE takes the form given by 3.9:

$$-\frac{\hbar^2}{2m}\nabla^2\psi(\mathbf{r}) + V(\mathbf{r})\psi(\mathbf{r}) = E\psi(\mathbf{r}) \tag{3.9}$$

The equation is fundamentally a wave equation, describing how the quantum state of a physical system evolves over time. It's commonly written in two forms: the time-

dependent Schrödinger equation (TDSE) and the time-independent Schrödinger equation (TISE). The time-independent Schrödinger equation (TISE) is derived from the TDSE under certain conditions and is used to find the stationary states of a quantum system. These states have well-defined energies and do not evolve in time.

3.3.3 Continuity Equation

The continuity equation in semiconductor physics describes the conservation of charge carriers within a semiconductor material. It's expressed mathematically as:

$$\frac{\partial \rho}{\partial t} + \nabla \cdot \mathbf{J} = S \tag{3.10}$$

where:

- ρ represents the charge carrier density,
- t is time,
- $\mathbf{J}$ is the current density vector,
- $\nabla\cdot$ denotes the divergence operator,
- S represents any sources or sinks of charge carriers.

This equation ensures that any change in the charge carrier density over time ($\frac{\partial \rho}{\partial t}$) is balanced by the divergence of the current density ($\nabla \cdot \mathbf{J}$) and any external sources or sinks of charge carriers (S).

At equilibrium point the current density is expressed as:

$$J = q\mu_n n \nabla \cdot E_{F_n} \tag{3.11}$$

where E_{F_n} is quasi-Fermi level for electrons.By substituting 3.11 into 3.10 we get

$$\nabla \cdot (\mu_n n \nabla E_{F_n}) = 0 \tag{3.12}$$

3.3.4 Carrier density

For a 2D electron gas, such as at the interface of two semiconductor materials, the carrier density is given by 3.13:

$$n = \frac{2mk_BT}{\pi\hbar^2}\left[1 + \exp\left(\frac{E_F - E_i}{k_BT}\right)\right] \tag{3.13}$$

The carrier density in a 2DEG is governed by quantum mechanical principles and can be described using the Fermi-Dirac statistics, which characterize the behavior of fermions (such as electrons) at finite temperature. This equation describes how the carrier density changes with temperature and chemical potential. At higher temperatures, more electrons are excited to higher energy states, leading to an increase in carrier density. The chemical potential represents the energy required to add an electron to the system, and its variation can influence the carrier density. The carrier density in a 2DEG is crucial in understanding and designing semiconductor devices such as field-effect transistors (FETs), where the behavior of electrons in the 2DEG determines device performance. By controlling the carrier density through external means such as gate voltages, researchers can manipulate the conductivity and other electronic properties of semiconductor devices.

3.4 Numerical Methods:

3.4.1 Newton's Method

Newton's method is an iterative numerical technique used to find the roots of a real-valued function $f(x)$. It starts with an initial guess x_0 and iteratively improves the estimate until a desired level of accuracy is reached. The iterative formula is given by 3.14:

$$x_{n+1} = x_n - \frac{f(x_n)}{f'(x_n)} \tag{3.14}$$

where $f'(x_n)$ is the derivative of $f(x)$ with respect to x.

3.4.2 Finite Element Method

The finite element method (FEM) is a numerical technique used to approximate solutions to differential equations by dividing the domain into smaller, simpler elements. It is widely used in engineering and physics for problems involving structural analysis, heat transfer, fluid dynamics, and electromagnetics.

In FEM, the domain is discretized into finite elements, and the governing differential equations are approximated over each element. The resulting system of algebraic equations is then solved to obtain the solution across the entire domain.

3.4.3 Gradient Clipping:

Consider the iterative update rule for a variable x_i:

$$x_i^{\text{new}} = x_i + \Delta x_i, \tag{3.15}$$

where Δx_i is the computed change.

To prevent excessively large updates, we apply gradient clipping:

$$\Delta x_i^{\text{clipped}} = \max\left(-\Delta x_{\max}, \min\left(\Delta x_i, \Delta x_{\max}\right)\right), \tag{3.16}$$

where $\Delta x_{\max}$ is a predefined threshold.

The variable is then updated using the clipped gradient:

$$x_i = x_i + \Delta x_i^{\text{clipped}}. \tag{3.17}$$

By limiting Δx_i, gradient clipping prevents large, destabilizing steps, promoting smooth convergence towards the solution. This technique enhances the robustness of iterative methods, especially for nonlinear or stiff differential equations.

(It should be noted that the algorithms described in Section 3.5 initially did not employ gradient clipping. This method was only implemented after observing the output curves in Figure 4.8, to achieve smoother convergence.)

3.5 Algorithms

3.5.1 First Simulation Approach:

The quantum-mechanical Schrödinger equation, which describes the distribution of electric charges, is intricately linked with the Poisson equation and the equations governing charge conservation. These equations, in turn, rely on probabilistic wave functions. Therefore, to accurately simulate HEMT devices, it is imperative to solve this system of equations in a self-consistent manner. Solving the Schrödinger equation yields energy eigenvalues and electron wave functions, enabling the determination of electron density. Subsequently, the electric field and potential distribution are extracted from the Pois-

son equation solution. When the charge conservation law is applied, it allows for the determination of Fermi surface distribution and current density within the device.The proposed algorithm is depicted in fig3.1 The algorithm must be executed adhering to

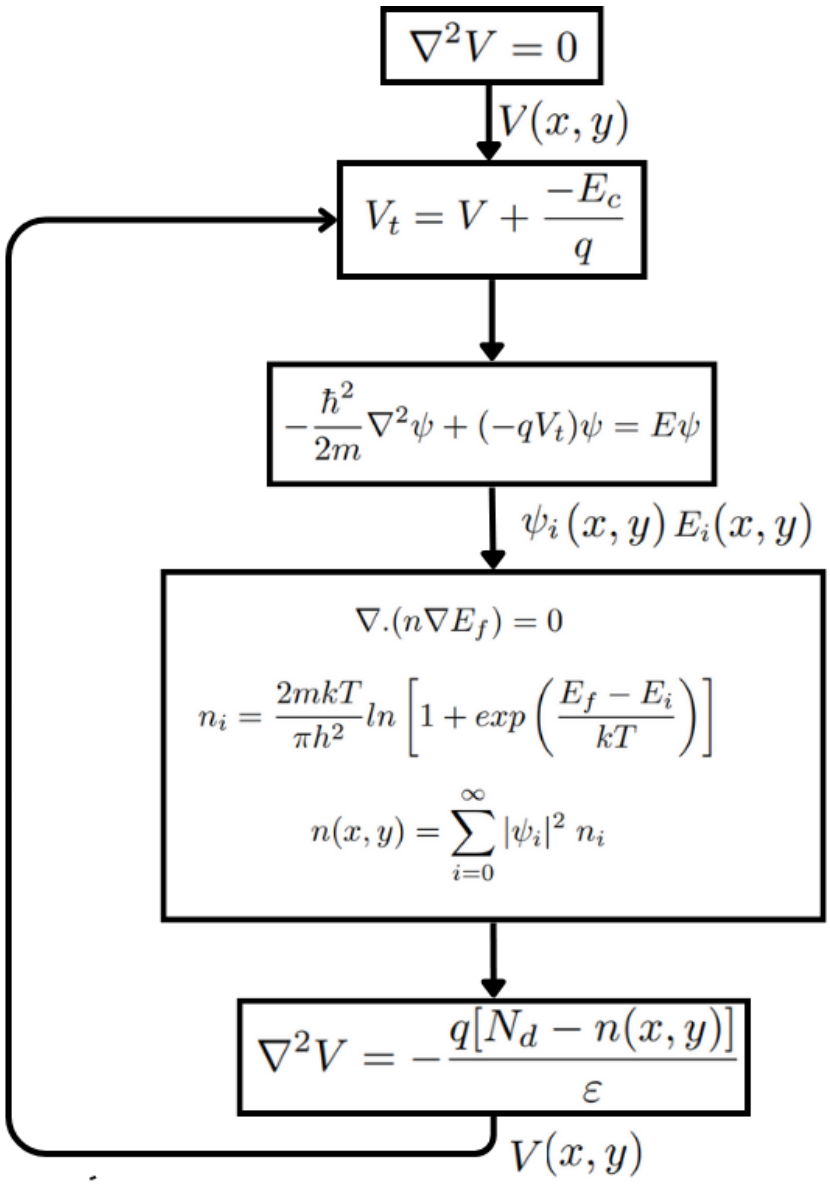

Fig. 3.1 Proposed algorithm for first simulation approach

the Dirichilet and Neumann boundary conditions enlisted in Fig 3.2(a). The proposed experimental structure on which the simulation was conducted is shown in Fig and the

dimensions have been enlisted in Fig 3.3.

Number	Details
1 (Drain)	$V = V_d, \psi = 0, E_f = -qV_d + \varphi_{ms}$
2 (Gate)	$V = V_g, \psi = 0, E_f = -qV_g + \varphi_{ms}, \frac{d}{dn}E_f = 0$
3 (Source)	$V = V_s, \psi = 0, E_f = -qV_s + \varphi_{ms}$
4	$\frac{d}{dn}V = 0, \psi = 0, \frac{d}{dn}E_f = 0$

W_1	W_2	W_3	W_4	l_D	l_G	l_{SU}	l_{SD}
20nm	28nm	15nm	10nm	30nm	20nm	5nm	5nm

(a)

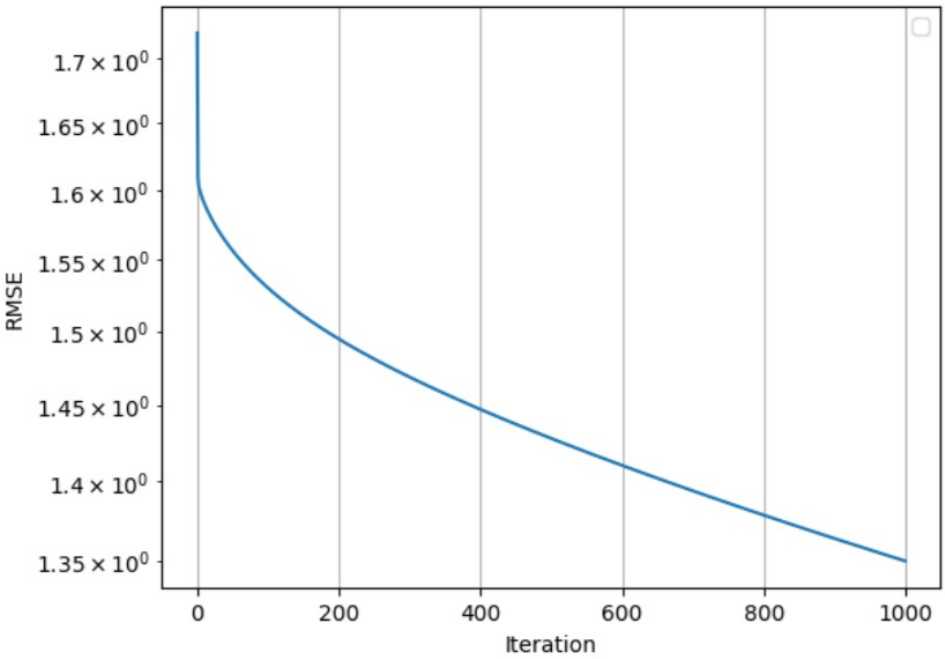

(b)

Fig. 3.2 (a) Boundary conditions and device dimensions, (b) RMSE loss curve

3.5.2 Second Simulation Approach:

In the second approach for the derivation of basic parameters in HEMTs, a nuanced consideration is given to the potential difference between the drain and source electrodes,

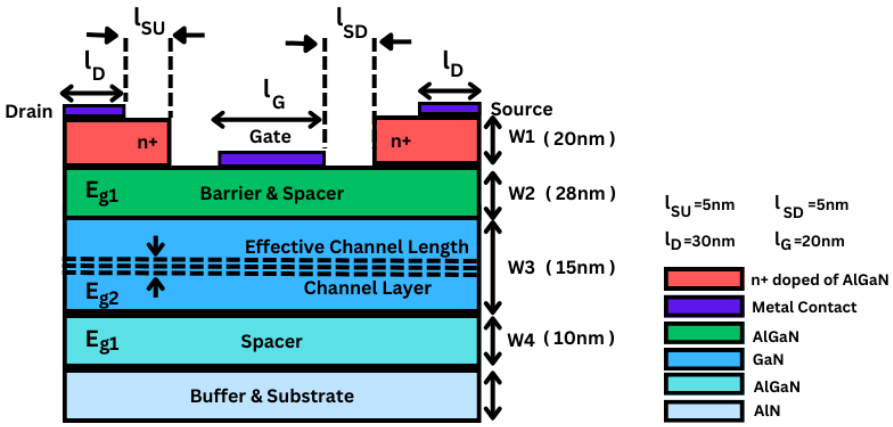

Fig. 3.3 Experimental HEMT structure used for this study

allowing for a thorough analysis of biased configurations. This approach accommodates the presence of a drain-source voltage (V_{DS}) and facilitates the examination of current density distribution within the transistor's bulk. The primary distinction between the non-equilibrium state (in the presence of V_{DS} and the equilibrium state (in the absence of V_{DS}) lies in the variation of the Fermi energy level. In the biased configuration, the Fermi energy level is no longer flat and constant; rather, it is replaced by the quasi-Fermi level. The quasi-Fermi energy levels at the source and drain contacts are determined by their respective applied voltages, while in other regions, they are derived from the continuity equation $\nabla.J = 0$, where J represents current density, n is carrier concentration, μ is electron mobility, and E_f is the quasi-Fermi level.

Furthermore, the electric field dependence of electron mobility ($\mu = \mu(E_{\text{eff}})$) is considered, introducing E_{eff} as the effective electric field. The mobility function is modeled through curve fitting to experimental data in GaN. Consequently, the mobility becomes a local function of coordinates, leading to Equation 3.18 which is a modified form of the continuity equation.

$$\nabla \cdot [\mu(x, y)n(x, y)\nabla E_f(x, y)] = 0. \tag{3.18}$$

The carrier concentration $n(x, y)$ is expressed in terms of the Fermi energy. This modification results in Equation 3.19 which is a nonlinear differential equation.

$$\nabla \cdot \left\{ \sum_{i=0}^{\infty} |\psi_i(x,y)|^2 \ln \left[1 + \frac{E_f - E_i}{kT} \right] \nabla E_f \right\} = 0, \tag{3.19}$$

which, upon solution, yields the Fermi level energy distribution throughout the transistor. The computation process, outlined in the flowchart shown in Fig. 3.4, involves solving this differential equation iteratively for each node, enabling the determination of $n(x, y)$ and the resulting current density at various points.

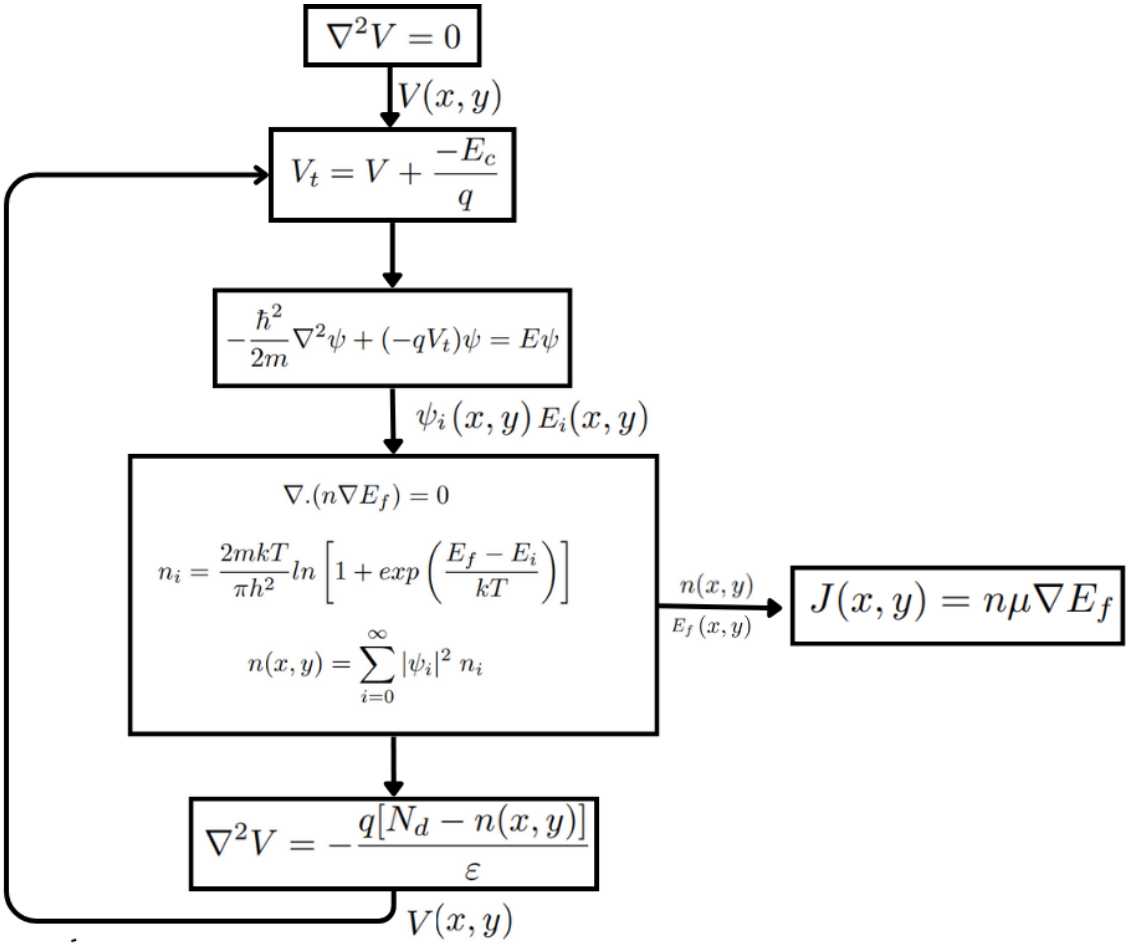

Fig. 3.4 Proposed algorithm for second simulation approach

Chapter 4

Results and Discussions

After running the algorithm, we have obtained crucial results that shed light on the behavior of High Electron Mobility Transistors (HEMTs). These results include the potential profiles across the device, the electron probability density distribution, and the electron density distribution across the device. The potential profiles provide insights into the electrostatics within the HEMT structure, revealing how the electric potential varies throughout the device. The electron probability density distribution offers information about the spatial distribution of electrons within the device, highlighting regions of higher and lower electron concentrations. Finally, the electron density distribution provides quantitative data on the number of electrons present at different positions within the HEMT, which is essential for understanding the device's electrical characteristics. These results serve as a foundation for further analysis and optimization of HEMT devices, contributing to advancements in high-frequency and high-power electronic applications. Additionally, they validate the accuracy and effectiveness of our simulation approach in capturing the intricate physics governing HEMT operation. The output graphs are as follows:

- fig 4.1 represents the potential variation across the device for the first simulation

approach.

- fig 4.2 represents the electron probability density across the device for the first simulation approach.
- fig 4.3 represents the electron density across the device, obtained after solving the first algorithm.
- fig 4.4 represents the electron density across the device obtained using the second approach
- fig 4.5 represents the potential across the device obtained from the second approach
- fig 4.6 represents the electron density across the device obtained using the second algorithm
- fig 4.7 represents the current density across the device
- fig 4.8 represents the IV characteristics obtained for the experimental structure in fig 3.3.

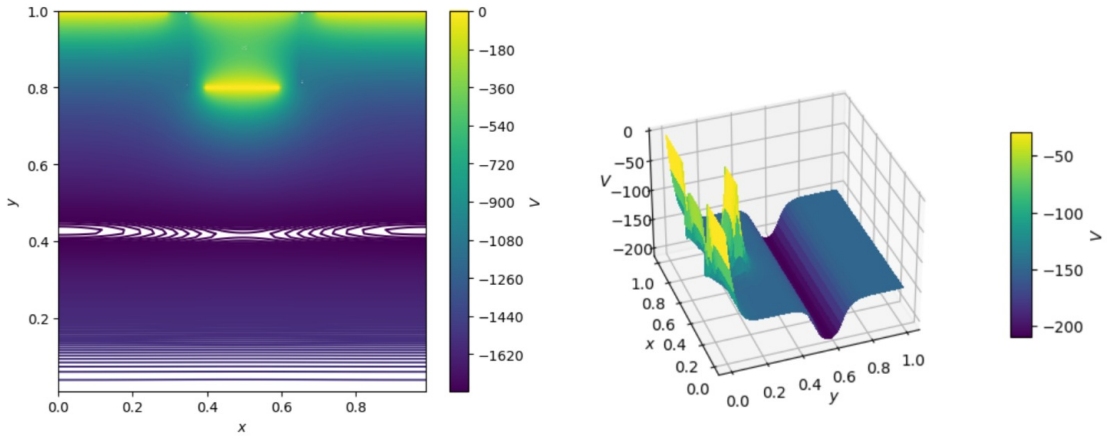

(a) 2D plot (b) 3D surface plot

Fig. 4.1 potential plots for first simulation approach

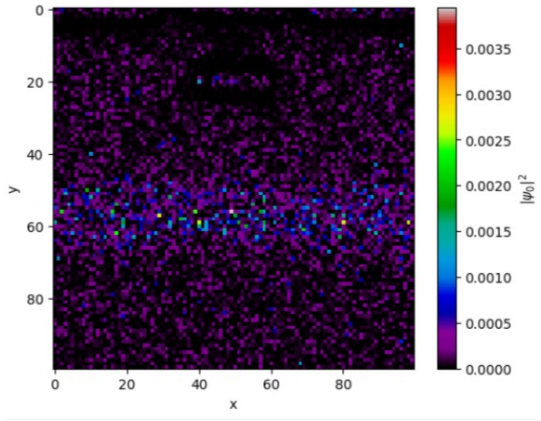

(a) ψ_0^2

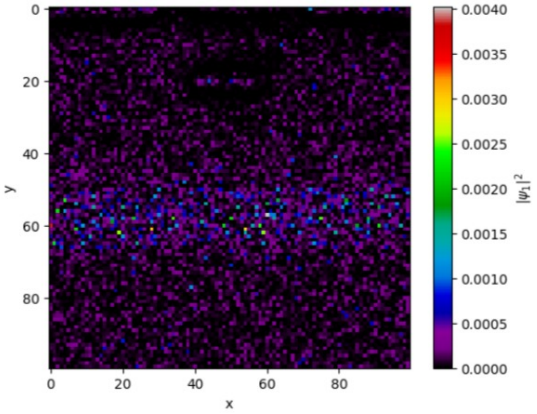

(b) ψ_1^2

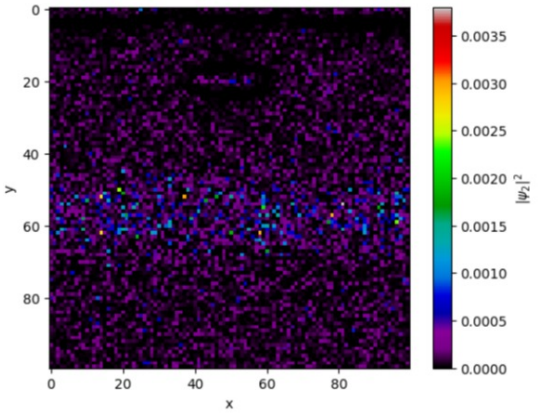

(c) ψ_2^2

Fig. 4.2 Probability density plots for electrons obtained using the first algorithm

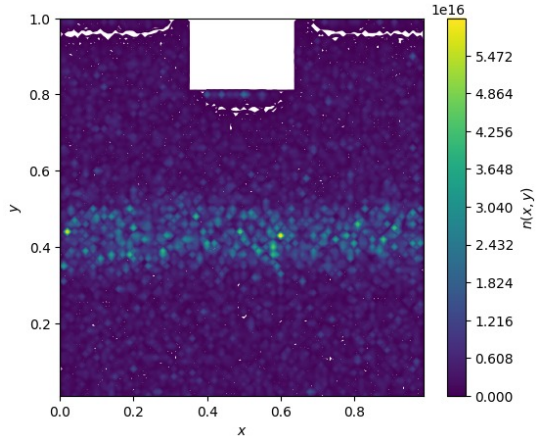

(a) 2D plot

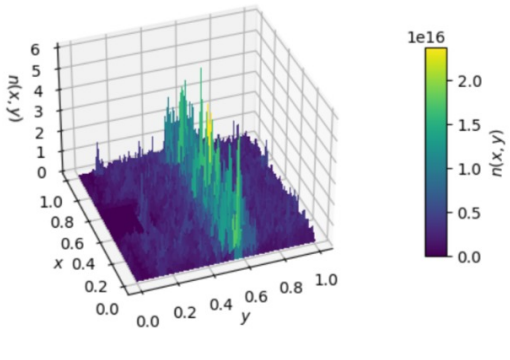

(b) 3D surface plot

Fig. 4.3 Electron density plots for the first algorithm

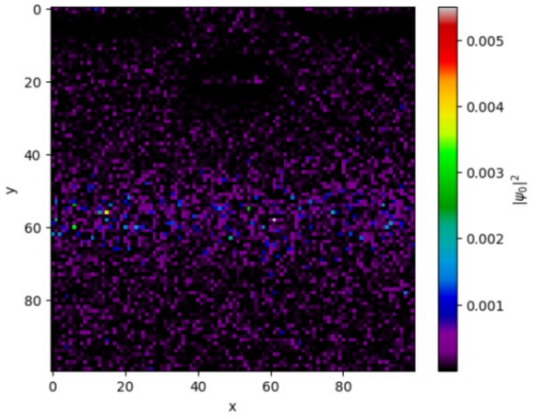

(a) ψ_0^2

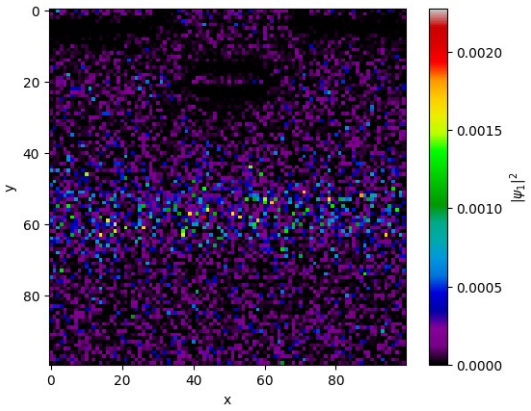

(b) ψ_1^2

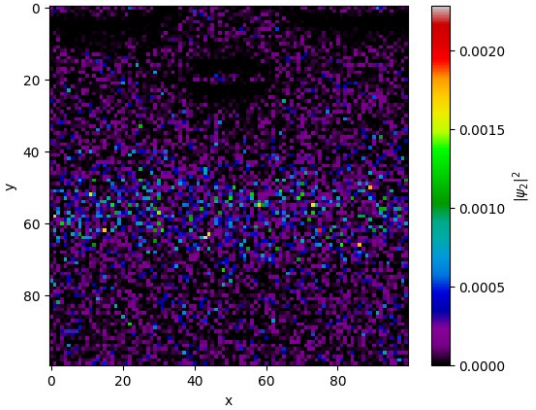

(c) ψ_2^2

Fig. 4.4 Probability density plots for electrons from 2nd algorithm

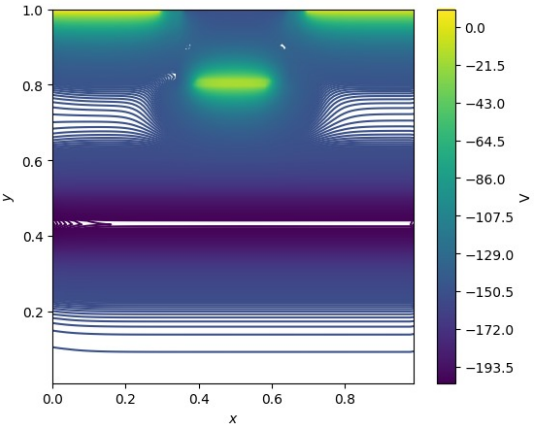

(a) 2D plot

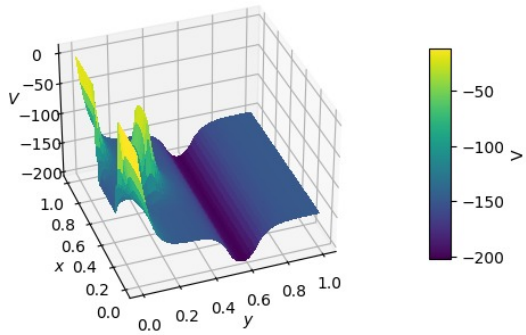

(b) 3D surface plot

Fig. 4.5 Potential plots from 2nd algorithm

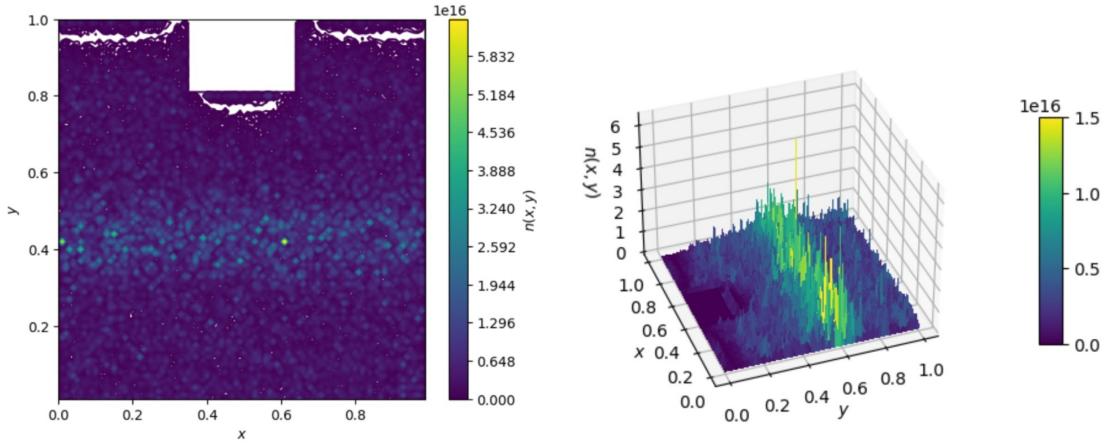

(a) 2D plot (b) 3D surface plot

Fig. 4.6 Electron density plots for the second algorithm

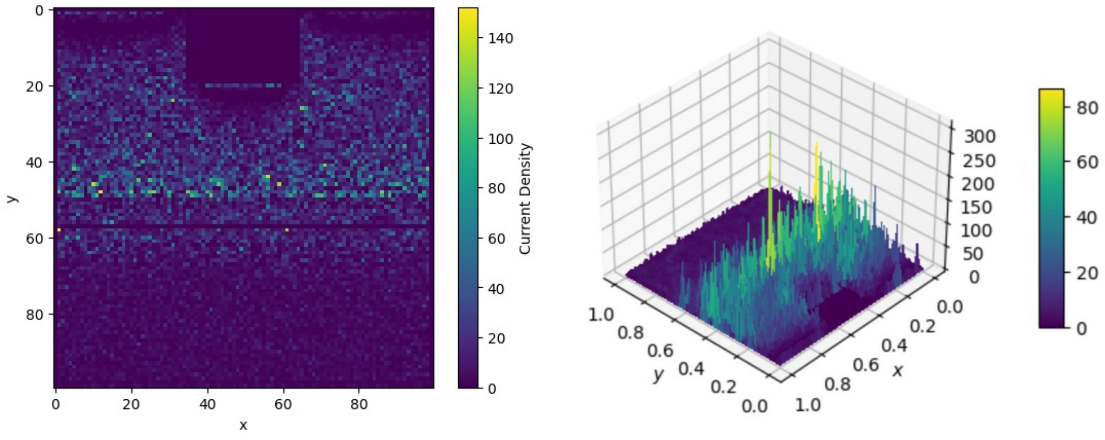

(a) 2D plot (b) 3D surface plot

Fig. 4.7 Current density plots from second algorithm

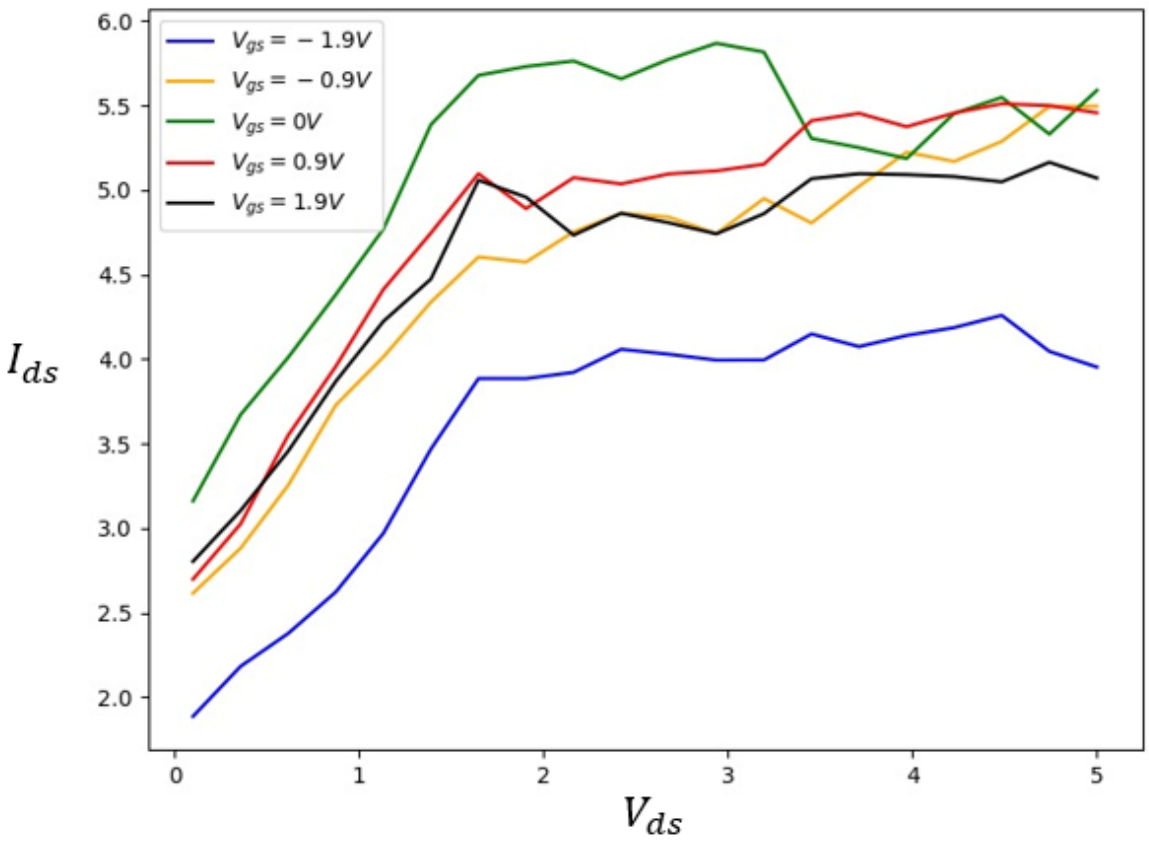

Fig. 4.8 I-V characteristics

Chapter 5

Comparison with state of the art

So far we have developed a simulator tailored for nanoelectronic heterojunction devices, leveraging physics-based equations such as Poisson's equation and Schrödinger's equation to accurately simulate the intricate behavior of HEMT (High Electron Mobility Transistor) structures. In the realm of device modeling, Silvaco TCAD stands out as a benchmark, renowned for its precision and comprehensiveness.

In our study, we conducted a thorough comparison between the output characteristics obtained from our proposed simulator and those derived from Silvaco TCAD for an identical HEMT structure. fig 5.3 visually represents this comparison, showcasing the similarities and differences between the two approaches.

To ensure alignment and consistency between the output curves generated by our Python-based simulator and those produced by Silvaco TCAD, we implemented a calibration process. This involved applying a scaling factor $c = 0.15$ to our simulator's output data.

The output plots derived from our simulator and Silvaco TCAD are depicted in fig. 5.1 and 5.1 respectively. Notably, both plots exhibit strikingly similar trends and patterns, underscoring the efficacy and reliability of our proposed simulation methodology.

This alignment further validates the robustness of our simulator in accurately capturing the complex behavior of nanoelectronic heterojunction devices, thereby offering valuable insights for device design and optimization.

In summary, our comparative analysis not only highlights the capabilities of our simulator but also underscores the importance of rigorous validation against industry-standard tools like Silvaco TCAD. This collaborative approach ensures confidence in our simulation results and contributes to advancements in the field of nanoelectronics.

A few points to consider here:

- The structure proposed in Fig. 3.3 operates at the nanometer scale, which inherently introduces challenges such as short channel effects. These effects can significantly impact the smoothness of the output characteristics, particularly when using low-density grids. The use of a 100x100 grid likely contributes to the observed irregularities in the output curves.

- To facilitate a meaningful comparison with Silvaco TCAD, we opted for a micrometer-scale structure. This decision was made to better emulate real-world conditions and to mitigate the impact of short channel effects. Additionally, we utilized a denser grid with a 1000 by 1000 NumPy matrix and applied gradient clipping. This denser grid provides a more detailed representation of the device characteristics, while gradient clipping ensures smoother convergence and results in smoother output curves. These enhancements improve the comparability between our simulator and Silvaco TCAD.

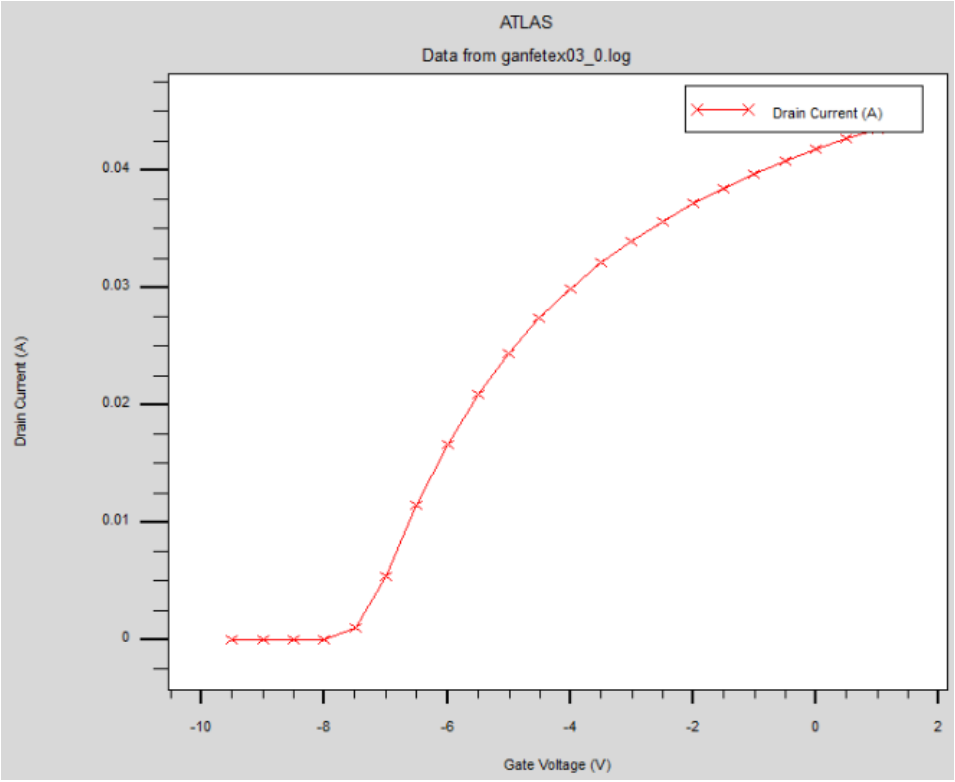

(a) I_{ds} vs V_{gs} Silvaco

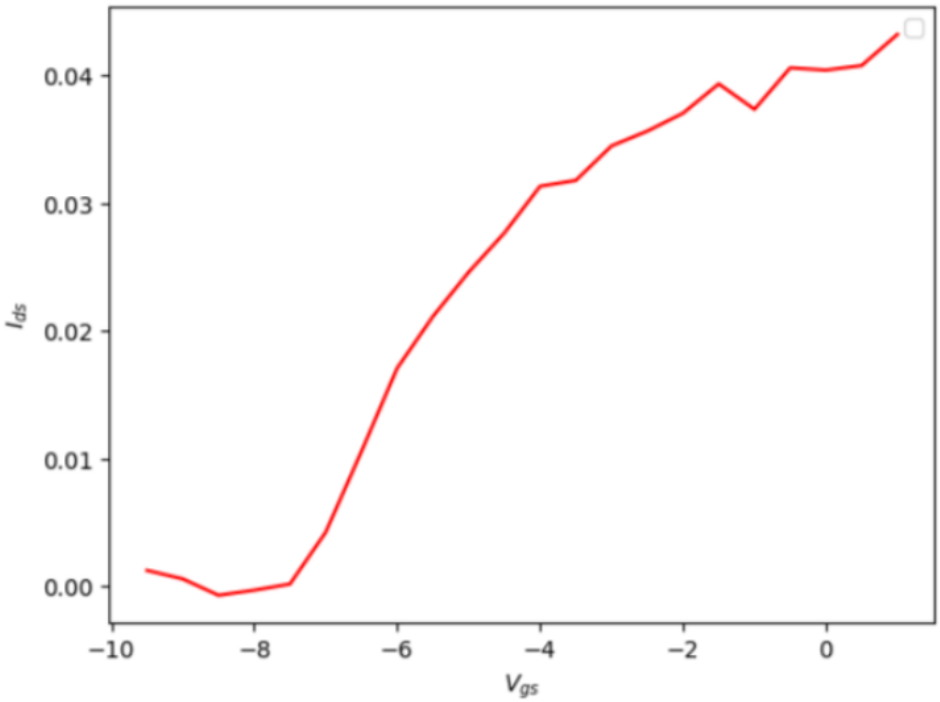

(b) I_{ds} vs V_{gs} proposed

Fig. 5.1 Comparison of I_{ds} vs V_{gs} plots

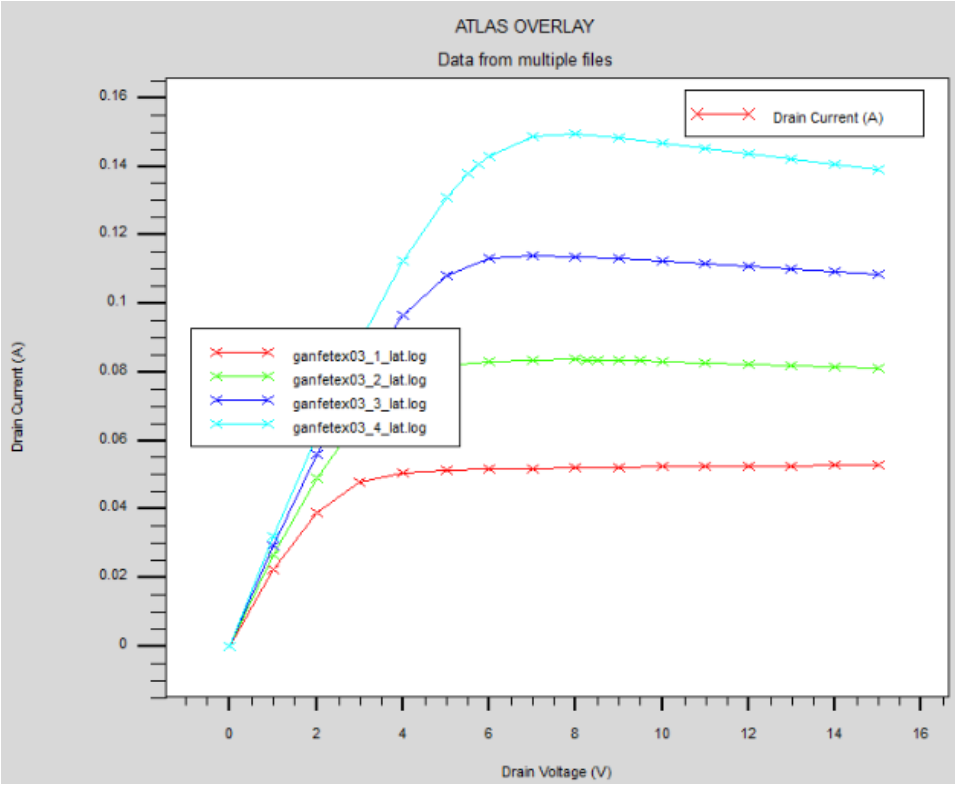

(a) I_{ds} vs V_{ds} Silvaco

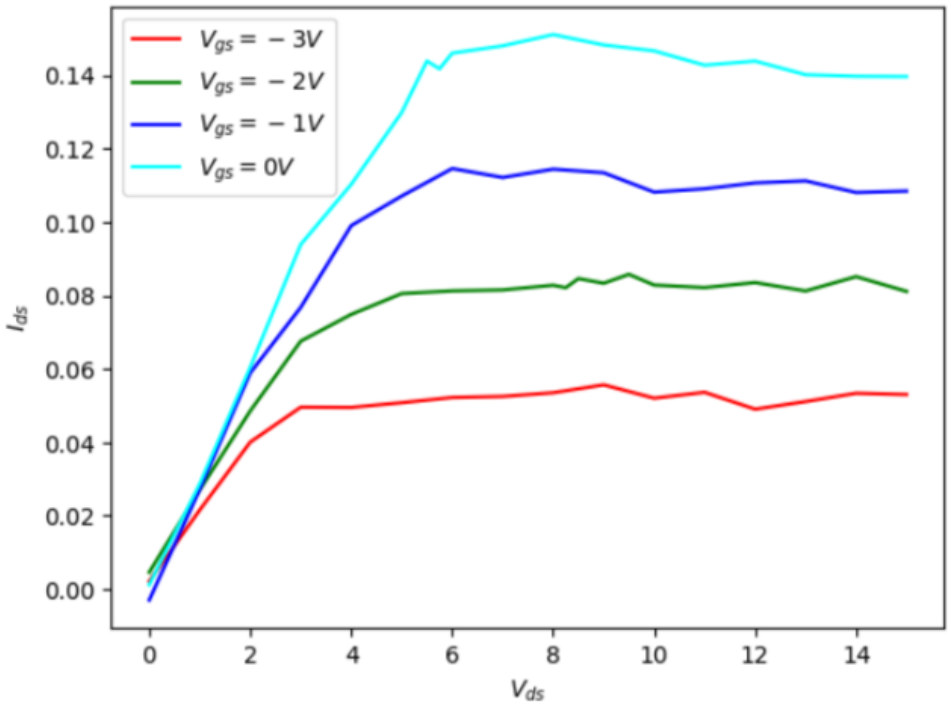

(b) I_{ds} vs V_{ds} proposed

Fig. 5.2 Comparison of I_{ds} vs V_{ds} plots

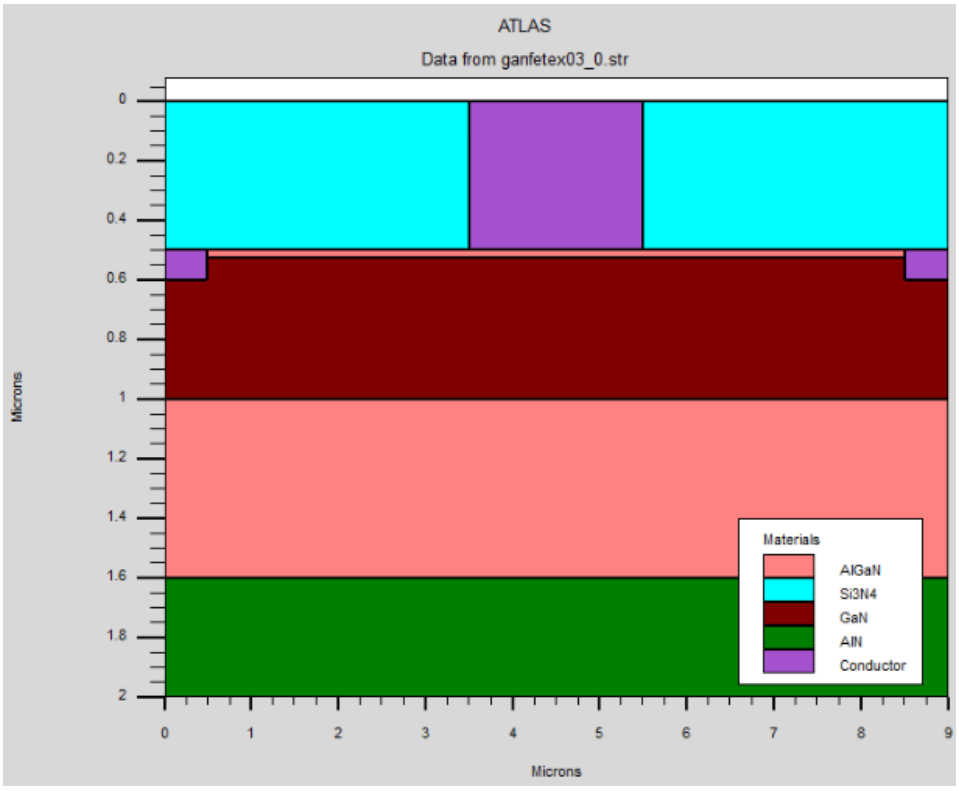

Fig. 5.3 Proposed structure for comparative analysis

Chapter 6

A Novel Nano-wire FET Structure

As observed in Chapter 5, our simulation approach performs comparably well to the state-of-the-art, as demonstrated by Silvaco TCAD. Notably, both plots exhibit strikingly similar trends and patterns, underscoring the efficacy and reliability of our proposed simulation methodology. However, it is important to note that the experimental structure previously used is not novel and is, at most, generic. In this chapter, we will leverage the insights gained from the previous experiments to develop a novel structure. The objective here is to optimize the I_{DS} versus V_{DS} characteristics.

6.1 Gate All Around FETs:

Gate-All-Around Field-Effect Transistors (GAA FETs) offer several advantages over traditional planar FETs, particularly in scaling and performance. One of the primary benefits is improved electrostatic control, which reduces short-channel effects and enhances the device's ability to suppress leakage currents, leading to better scalability for advanced nodes [6]. Additionally, GAA FETs exhibit superior drive current due to their ability to increase channel width without impacting the device's footprint, provid-

ing higher current densities and improved switching characteristics [7]. Moreover, the three-dimensional gate structure of GAA FETs surrounds the channel, offering more efficient gate control over the channel potential, which results in lower subthreshold swing and enhanced on-off current ratio. These advantages make GAA FETs a promising technology for future high-performance and low-power electronic devices.

6.2 Proposed Nanowire FET structure:

The Fig 6.1 illustrates a proposed gate-all-around (GAA) nanowire high electron mobility transistor (HEMT) structure. The central feature of the structure is the InN (indium nitride) nanowire, which is encased by a thin layer of GaN (Gallium nitride) that serves as a high-mobility channel material due to its superior electron transport properties. Surrounding the GaN layer is a gate dielectric made of SiO2 (silicon dioxide), which provides excellent insulation and minimizes gate leakage currents. The gate material itself is composed of a conductive layer, ensuring efficient gate control over the nanowire channel. Silicon serves as the substrate, with a layer of Si3N4 (silicon nitride) providing additional structural integrity and isolation. The intricate layering, as depicted, aims to maximize electron mobility and transconductance while minimizing short-channel effects and gate leakage, critical for the performance enhancements in next-generation high-frequency and high-power electronic devices.

6.3 Simulation Outputs on Silvaco:

The simulated I_{ds} vs. V_{ds} curves for various gate voltage (V_{g}) levels demonstrate the expected behavior of a Field-Effect Transistor (FET). As shown in Figure 6.3, the drain current (I_{ds}) increases with the drain-source voltage (V_{ds}) initially and then saturates, indicating the transition from the linear (ohmic) region to the saturation region.

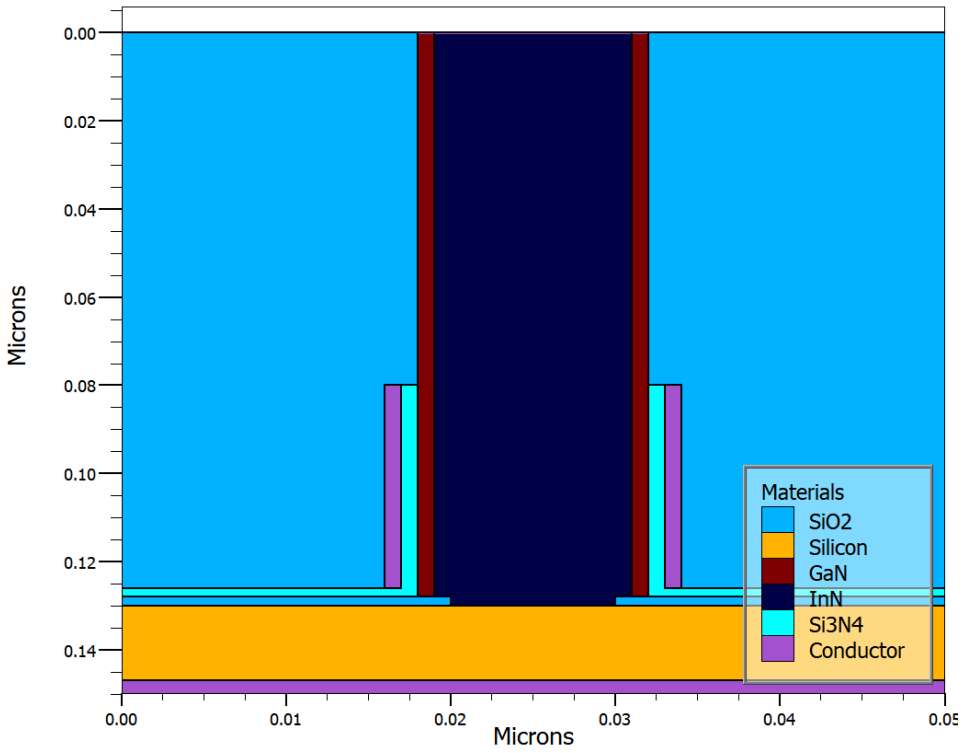

Fig. 6.1 Proposed novel gate all around FET structure

At lower V_g levels, the I_{ds} remains relatively low across the range of V_{ds} values, reflecting the reduced channel conductivity due to insufficient gate-induced electric field. As V_g increases, the channel conductivity improves, leading to higher I_{ds} values. This behavior is consistent with the enhancement mode operation of the FET, where a higher gate voltage induces a stronger electric field, enhancing the electron mobility and thereby increasing the drain current.

The I_{ds} vs. V_g curve for the novel FET structure, depicted in Figure 6.2, showcases the device's threshold voltage and transconductance characteristics. As V_g increases from 0V, the I_{ds} remains negligible until it surpasses the threshold voltage (V_{th}), beyond which a significant increase in I_{ds} is observed. This sharp rise indicates the formation of a conductive channel between the source and drain, typical of an enhancement mode FET.

The novel FET structure exhibits a well-defined threshold voltage, which is critical for low-power applications. Additionally, the steep I_{ds} increase post-threshold suggests a high transconductance, implying that the device can achieve substantial current modulation with minimal changes in gate voltage. This characteristic is highly desirable for high-speed and high-frequency applications.

Overall, the simulation results for both I_{ds} vs. V_{ds} and I_{ds} vs. V_g demonstrate the effectiveness of the novel FET structure in achieving high performance.

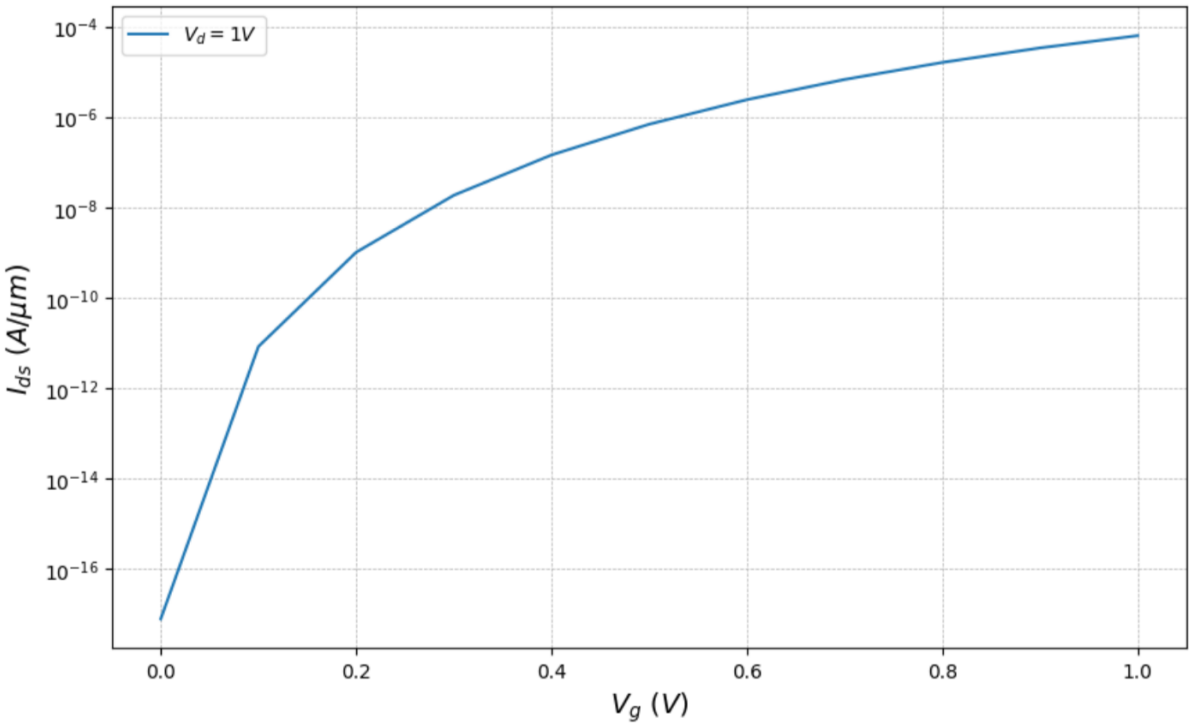

Fig. 6.2 I_{ds} vs V_{gs} simulation output for proposed novel structure on silvaco

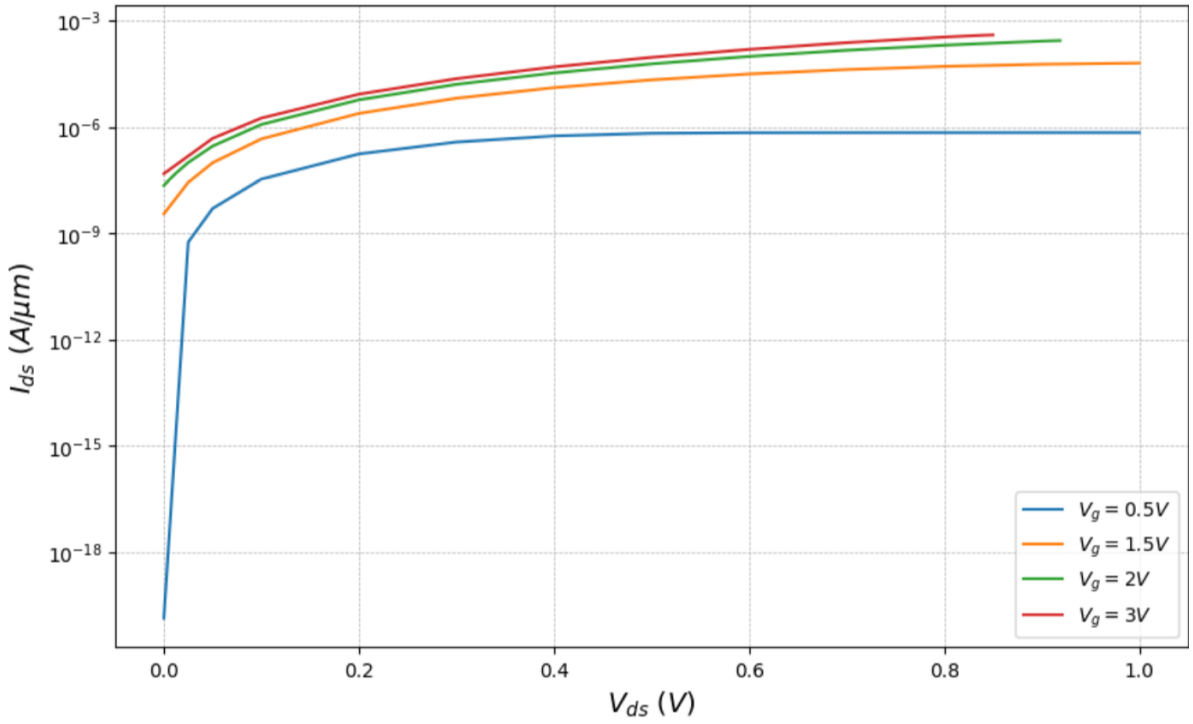

Fig. 6.3 I_{ds} vs V_{ds} simulation output for proposed novel structure on silvaco

Chapter 7

Conclusion

In conclusion, this report provides a comprehensive examination of High Electron Mobility Transistors (HEMTs), emphasizing the core principle of their operation: the formation of a two-dimensional electron gas (2DEG). HEMTs, crafted from Group III-nitride materials, are integral to high-power RF and microwave applications due to their unique ability to create a 2DEG at the heterointerface. This is achieved through the meticulous design of semiconductor layers with different bandgaps, resulting in a potential energy step that confines electrons within a two-dimensional plane.

The report introduces a cutting-edge simulation system that utilizes Kronecker matrices with convolution-based interpolation to solve the Poisson and Schrödinger equations self-consistently. This system provides detailed insights into various physical parameters of HEMTs, including electron wave functions, electric potential distribution, electron density, Fermi surface energy, and current density distribution.

The first phase of the project is predominantly mathematical, focusing on solving quantum mechanical equations to generate self-consistent solutions. In the subsequent phase, these insights are applied to develop a novel gate-all-around FET structure, with simulation results obtained using Silvaco TCAD. This research substantially enhances our understanding and optimization of HEMTs, paving the way for advanced nanoscale

electronic applications.

References

[1] Donald A Neamen. *emiconductor Physics and Devices Basic Principles*. Tata McGraw Hill Publishing, 1992.

[2] Hadis Morkoç. *Handbook of Nitride Semiconductors and Devices, Electronic and Optical Processes in Nitrides*. John Wiley & Sons, 2009.

[3] Zarak Bhat and Sheikh Aamir Ahsan. Physics-based analytical modeling of p-gan/algan/gan hemts. In *2022 IEEE 19th India Council International Conference (INDICON)*, pages 1–6. IEEE, 2022.

[4] R Singh, TR Lenka, DK Panda, HPT Nguyen, N El I Boukortt, and G Crupi. Analytical modeling of i–v characteristics using 2d poisson equations in aln/β-ga2o3 hemt. *Materials Science in Semiconductor Processing*, 145:106627, 2022.

[5] G Leuzzi. *Simulation of GaN/AlGaN heterostructures for a HEMT simulator*. PhD thesis, UNIVERSITY of L'AQUILA, 2011.

[6] Wei Hu and Feng Li. Scaling beyond 7nm node: An overview of gate-all-around fets. In *2021 9th international symposium on next generation electronics (ISNE)*, pages 1–6. IEEE, 2021.

[7] Soyoun Kim, Kitae Lee, Sihyun Kim, Munhyeon Kim, Jong-Ho Lee, Sangwan Kim, and Byung-Gook Park. Investigation of device performance for fin angle optimization

in finfet and gate-all-around fets for 3 nm-node and beyond. *IEEE Transactions on Electron Devices*, 69(4):2088–2093, 2022.